Quarterly Progress Report

Technical and Financial

Deep Water Ocean Acoustics
Award No.: N00014-14-C-0172

Report No. QSR-14C0172-Ocean Acoustics-093016
Prepared for: Office of Naval Research
For the period: July 1, 2016 to September 30, 2016

Submitted by:
Principal Investigator/Author: Kevin Heaney
Ocean Acoustical Services and Instrumentation Systems, Inc.
5 Militia Drive
Lexington, MA 02421

Date Submitted: October 7, 2016

Notices:

Table of Content

Technical Progress Report

1. Introduction

The goal of this research is to increase our understanding of the impact of the ocean and seafloor environmental variability on deep-water (long-range) ocean acoustic propagation and to develop methodologies for including this in acoustic models. Experimental analysis is combined with model development to isolate specific physics and improve our understanding. During the past few years, the physics effects studied have been three-dimensional propagation on global scales, deep water ambient noise, under-ice scattering, bathymetric diffraction and the application of the ocean acoustic Parabolic Equation to infrasound.

2. Tasks

a. Task 1: Basin Scale Acoustic Propagation and CTBTO Data Analysis

The Parabolic Equation Model Peregrine, was applied to observations made at the United Nations Comprehensive Test Ban Treaty Organization (CTBTO) of a set of 100 shots deployed off of the coast of Japan. These measurements were made by Prof. Tomoaki Yamada, from the University of Tokyo. This work is also in collaboration with Dr. Mario Zampolli and Dr. Georgious Haralabulus of the CTBTO. These were recorded over 190000 km away at the Juan Fernandez receiver site (HA03). The 3D PE was run, using reciprocity, from Juan Fernandez, Chile to each shot location off the coast of Japan. Peregrine has an option where the 3D code can be computed along a tube centered on the geodesic path. Initially this computational tube was set to 300km, as it was expected that the energy received in the shadow of Hawaii would refract around small islands and fill in the shadow. This turned out not to be the case. The energy observed in the shadow of the Hawaiian Islands is refracted from Midway, and thus the width of the computational tube must be set to 1000 km. The 2D / 3D global run, incoherently averaged (in Intensity) from 4 to 20 Hz for a receiver depth of 30-90m is shown in Figure 1. The persistence of shadows in the 2D plot (upper panel) is the primary difference. There are 3 places where significant bathymetric interaction occurs and 3D diffraction dominates. The first is the South East Pacific Rise, just northwest of Juan Fernandez at a Latitude of roughly 28°S. The second is the Hawaiian Island Chain, extending to Midway Island at 28°N, 177°W and finally the Emperor Seamount chain running due north at 170°E. The effect of these bathymetric interactions is to fill the shadow zone completely by the time the Asian continent is encountered at the Japan coastline.

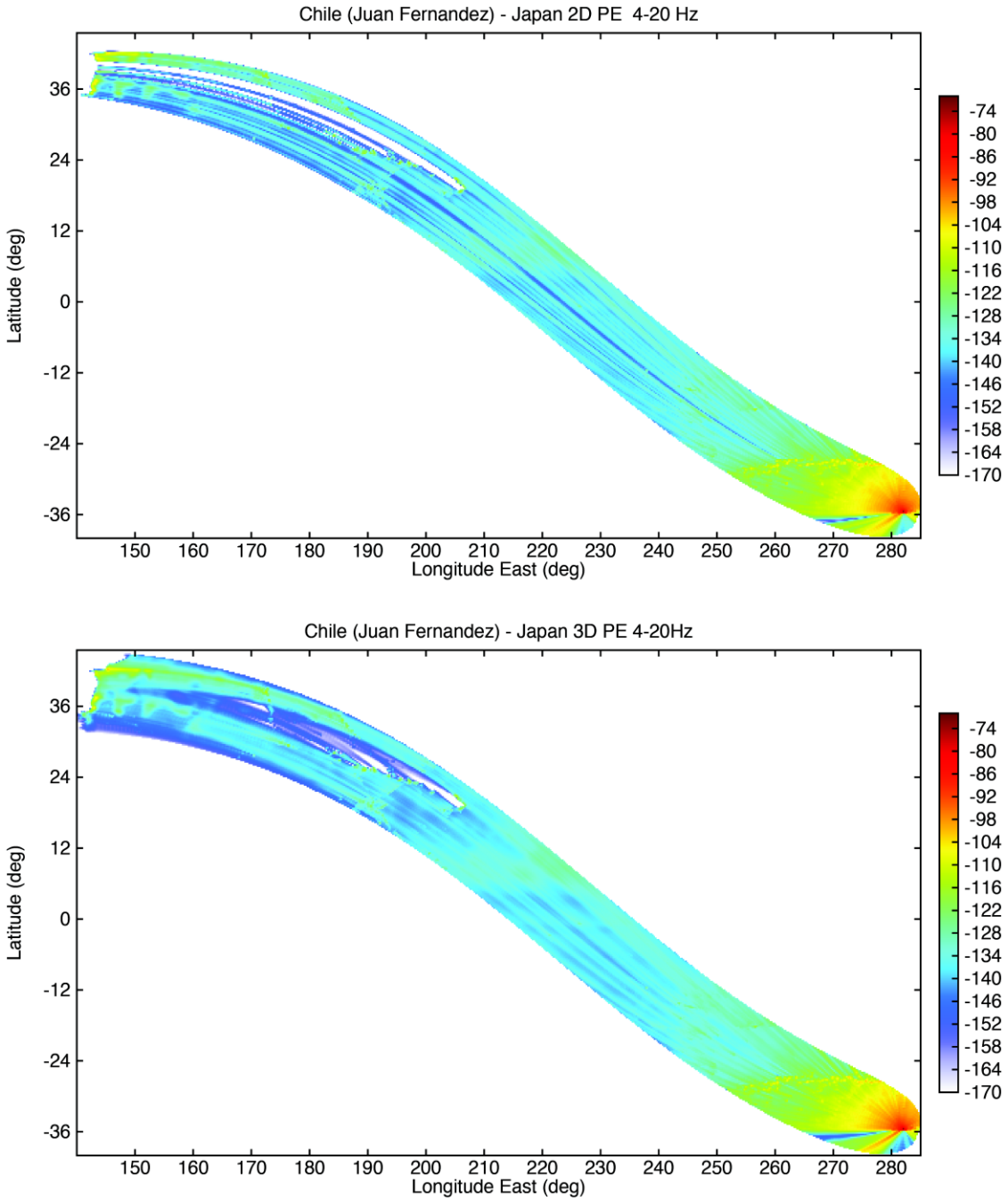

Figure 1. Broadband incoherent TL (4-20Hz) computed using the two-dimensional (top) and three-dimensional (bottom) Parabolic Equation (Peregrine) from Juan Fernandez (of Chile) to the Japanese Coast.

b. Task 2: Passive Acoustic Thermometry

From theoretical considerations it follows that the acoustic traveltime between two sensors can be obtained from the ambient noise field. In underwater acoustics, this

traveltime strongly depends on the depth and temperature and to a lesser extent on salinity (Dushaw et al. 2009). In order to apply this theory in long range ocean acoustics and derive deep ocean temperature, hydro-acoustic recordings from a station near Ascension Island are analyzed. This station, called H10, is in place for the verification of the Comprehensive Nuclear-Test-Ban Treaty and as such part of the International Monitoring System (IMS). H10 consists of two hydrophone triplets which are placed in the Sound Fixing and Ranging (SOFAR) channel (Dahlman et al. 2009). The SOFAR channel is a low-velocity layer in the deep ocean, i.e., the average channel axis depth is 1.5 km, which allows low frequency sound to be detected over long ranges (Munk & Forbes 1989). The efficiency of the SOFAR channel for sound propagation has already been used in studies related to earthquakes (Evers at al. 2004; De Groot-Hedlin 2005; Guilbert et al. 2005), icebergs (Chapp, Bohnenstiel & Tolstoy 2005; Talandier et al. 2006; Evers et al. 2013), explosions (Munk & Forbes 1989; Prior et al. 2011), marine mammals (Prior et al. 2012) and underwater volcanoes (Green at al. 2013). Guided wave propagation contributes to the limited acoustical attenuation by the SOFAR channel. In this study, the triplets are considered as arrays which are located to the north (7.84◦S, 14.49◦W) and south (8.95◦S,14.65◦W) of Ascension Island, at an inter-array distance of about 126 km, to avoid blocking by the island for sound coming from certain directions (see Figure 2).

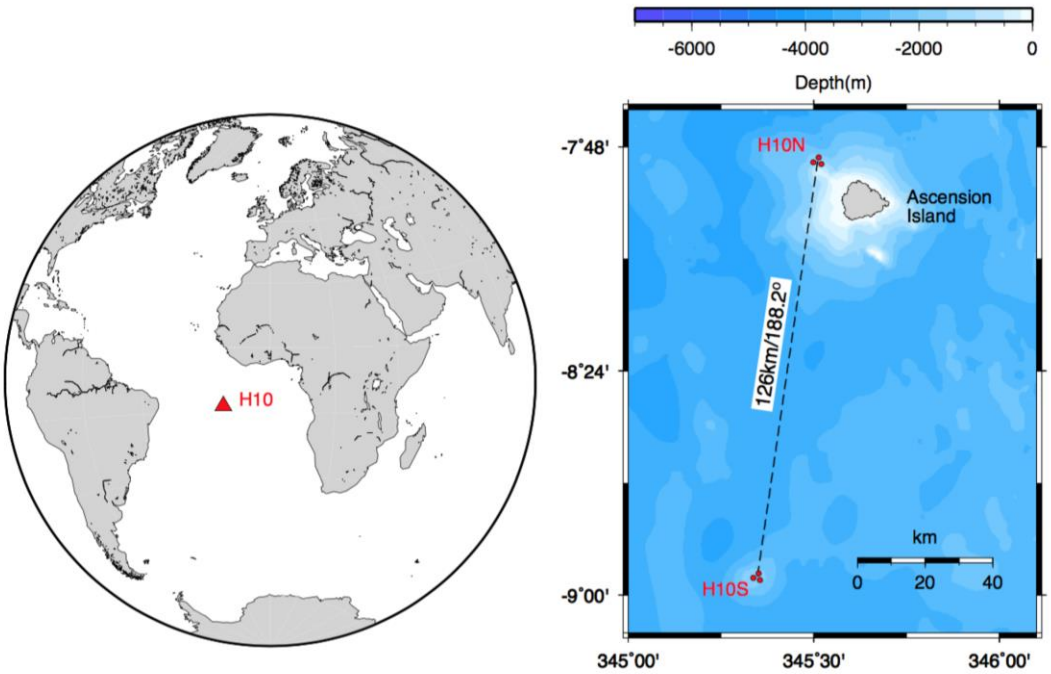

Figure 2. The location of H10 in the Atlantic Ocean near Ascension Island. H10 consists of two three-element hydrophone arrays, one to the north (H10N) and one to the south (H10S) of Ascension Island. The aperture of each array is about 2 km. The distance between the arrays is 126 km and the bearing connecting the two arrays is 188.2°.

Figure 3 shows the cross correlation results for a frequency of 0.5 to 15 Hz for 2011, May 5 between 11h and 12h UTC. The raw unfiltered recordings of N2 and S2 are also shown. It has been tested that this arbitrarily chosen day and hour are representative. The

envelopes are calculated to accurately measure the peak of the cross correlation. It follows from Figure 3 that cross correlations for this day have coefficients up to 0.4. Significant cross correlation coefficients start to be retrieved from a frequency of 3 Hz and higher, which corresponds to the frequencies which the SOFAR channel can facilitate due to its limited thickness. Patches of energy in specific frequency bands appear more correlated than those in other frequency bands, which is typical for the modal propagation in the SOFAR channel (De Groot-Hedlin, Blackman & Jenkins 2009). As expected, the width of the envelope reduces with increasing frequency, enabling a higher time resolution. Furthermore, the lag time becomes smaller with increasing frequency. This can be understood by taking into account the shape of the SOFAR channel, where the lowest sound speed is at the channel axis. The smaller the wavenumber, the more the horizontal propagation energy is confined to the channel axis, which results in the larger lag times. As the frequency increases, more of the energy gets guided by the higher sound speeds surrounding the channel axis. In a ray-theoretical approach, the latter corresponds to rays being less horizontally incident on the receivers with increasing frequency. In this specific example, the difference in the lag time is 0.3 seconds, i.e., 85.5s at 4.3 Hz and 85.2s at 7.5 Hz.

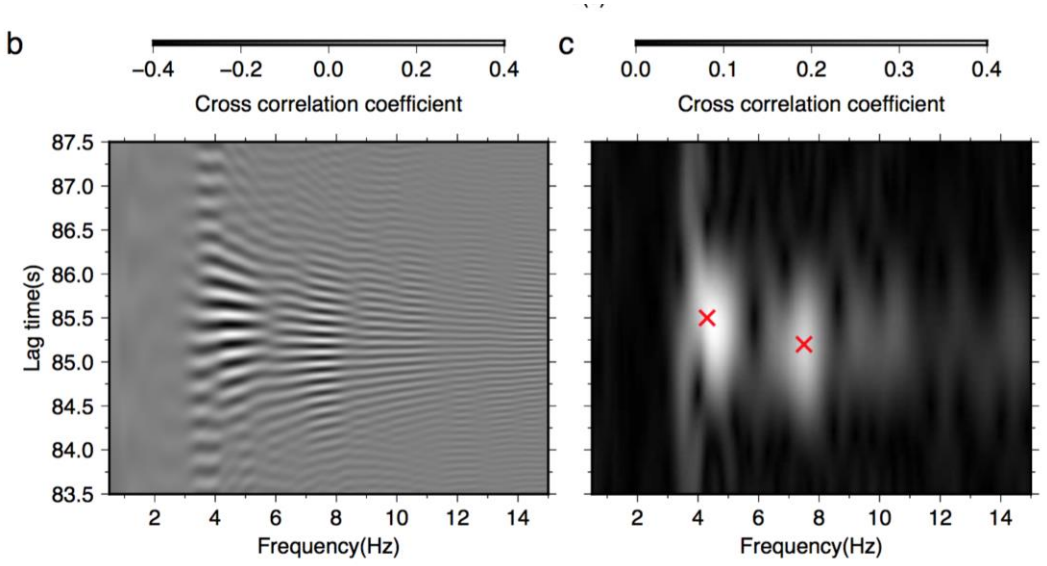

Figure 3. The cross correlation coefficients between N2 and S2 are shown for both (b) the cross correlation and (c) the envelop surrounding the cross correlation. These results are obtained with frequency bands of 1.0 Hz and a sliding window with steps of 0.1 Hz. The maxima (red crosses) are determined as 85.5s at 4.3 Hz and 85.2s at 7.5 Hz.

The Parabolic Equation Model (Peregrine) was used to model the impulse response (Green's Function) between the two receivers N2 and S2 for a 3-5Hz signal and a 5-10Hz signal. This propagation effort revealed that the ETOPO1 bathymetry model had significant difficulties (as the S2 receiver was actually deeper than the ETOPO reported bathymetry, which must be incorrect). The modeled arrival times do not quite match the observed 85.5 and 85.2 Hz, but the higher frequency model is 0.3 s faster than the lower

frequency. Possibly there is an error in the range due to either the geodesic correction or the element positioning.

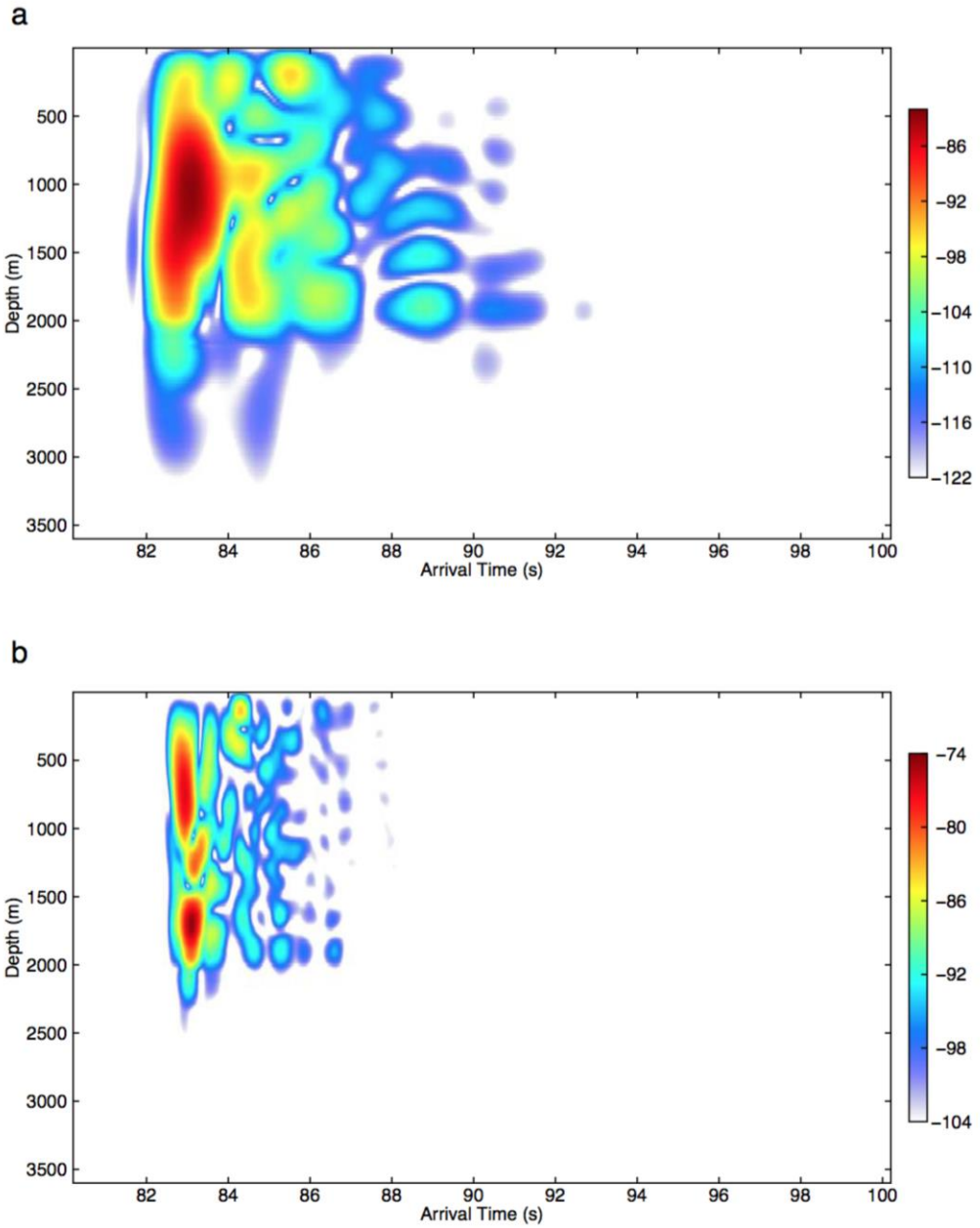

Figure 3. The travel time between N1 and S1 obtained from modeling with the parabolic equation. Results are shown for (a) the low frequency band of 3 to 5 Hz and (b) the high frequency band of 5 to 10 Hz.

3. Future Plans

Dr. Heaney plans to write up the model data comparisons for the Japan Seismic Tomography shot recordings on the Juan Fernandez CTBTO station.

4. Publications and Peer Interactions

Dr. Heaney submitted a paper, as a co-author with Dr. Laslo Evers of KNMI (The Dutch Meteorological Institute) to the Geophysical Journal International entitled: *"Deep ocean sound speed characteristics passively derived from the ambient acoustic noise field".*

Revisions were made to "Bathymetric diffraction of basin-scale hydroacoustic signals" by Kevin D. Heaney, Richard L. Campbell and Mark Prior, and it was re-submitted to Journal of the Acoustical Society of America on August 30, 2016.

5. References

Brown, M. G., Godin, O. A., Williams, N. J., Zabotin, N. A., Zabotina, L., & Banker, G. J., 2014. Acoustic Green's function extraction from ambient noise in a coastal ocean environment, *Geophys. Res. Lett.*, 41, 5555–5562.

Chapp, E., Bohnenstiel, D. R., & Tolstoy, M., 2005. Sound-channel observations of ice-generated tremor in the Indian Ocean, *Geochemistry Geophysics Geosystems*, 6, Q06003.

Chen, X. & Tung, K. K., 2014. Varying planetary heat sink led to global-warming slowdown and acceleration, *Science*, 345, 897–903.

Collins, M. D., 1993. A split-step Pade´ solution for the parabolic equation method, *J. Acoust. Soc. Am.*, 93, 1736–1742.

Dahlman, O., Mykkeltveit, S., & Haak, H., 2009. *Nuclear Test Ban*, Springer.

De Groot-Hedlin, C., Blackman, D. K., & Jenkins, C. S., 2009. Effects of variability associated with the Antarctic circumpolar current on sound propagation in the ocean, *Geophys. J. Int.*, 176, 478–490.

De Groot-Hedlin, C. D., 2005. Estimation of the rupture length and velocity of the Great Sumatra earthquake of Dec 26, 2004 using hydroacoustic signals, *Geophys. Res. Lett.*, 32, L11303.

Dushaw, B. D., Worcester, P. F., Munk, W. H., Spindel, R. C., Mercer, J. A., Howe, B. M., Metzger, K., Birdsall, T. G., Andrew, R. K., Dzieciuch, M. A., Cornuelle, B. D., & Menemenlis, D., 2009. A decade of acoustic thermometry in the North Pacific Ocean, *J. Geophys. Res.*, 114, C07021.

Evers, L. G. & Snellen, M., 2015. Passive probing of the sound fixing and ranging channel with hydro-acoustic observations from ridge earthquakes, *J. Acoust. Soc. Am.*, 137, 2124–2136.

Evers, L. G., Green, D. N., Young, N. W., & Snellen, M., 2013. Remote hydroacoustic sensing of large icebergs in the southern Indian Ocean: Implications for iceberg monitoring, *Geophys. Res. Lett.*, 40, 4694–4699.

Evers, L. G., Brown, D., Heaney, K. D., Assink, J. D., Smets, P. S. M., & Snellen, M., 2014. Evanescent wave coupling in a geophysical system: Airborne acoustic signals from the mw 8.1 Macquarie Ridge earthquake, *Geophys. Res. Lett.*, 41, 1644–1650.

Green, D. N., Evers, L. G., Fee, D., Matoza, R. S., Snellen, M., Smets, P., & Simons, D., 2013. Hydroacoustic, infrasonic and seismic monitoring of the submarine eruptive activity and sub-aerial plume generation at South Sarigan, May 2010, *J. Volc. and Geothermal Res.*, 257, 31–43.

Guilbert, J., Vergoz, J., Schissele´, E., Roueff, A., & Cansi, Y., 2005. Use of hydroacoustic and seismic arrays to observe rupture propagation and source extent of the Mw = 9.0 Sumatra earthquake, *Geophys. Res. Lett.*, 32, L15310.

6. Financial Summary

OASIS, INC.
JOB STATUS REPORT **9/30/2016**

1172 DEEP WATER ACOUSTICS **N00014-114-C-0172**
POP: 9/27/13-12/30/16

CONTRACT VALUE	Cost	Fee	Total
Contract Value	$368,935	$27,048	$395,983
Funding Value:	**$368,935**	**$27,048**	**$395,983**
Remaining to Fund:	$0	$0	$0

CUMULATIVE SPENDING WITH COMMITMENTS

	DIRECT	OH	MH	TOTL COST	FEE	**TOTAL**
ACTUAL						
OASIS	$204,919	$152,077	$4,487.13	$361,484	$27,111	**$388,595**
COMMITTED						
	$0	$0	$0	$0	$0	**$0**
	$204,919	$152,077	$4,487	$361,484	$27,111	**$388,595**
TOTAL REMAINING TO SPEND:						**$7,388**